Radial compression and torque-balanced steady states of single-component plasmas in Penning-Malmberg traps[a]

J. R. Danielson[b] and C. M. Surko
Department of Physics, University of California at San Diego, La Jolla, California 92093

Penning-Malmberg traps provide an excellent method to confine single-component plasmas. Specially tailored, high-density plasmas can be created in these devices by the application of azimuthally phased rf fields (i.e., the so-called "rotating wall" technique). Recently, we reported a regime of compression of electron (or positron) plasmas in which the plasma density increases until the $E \times B$ rotation frequency, ω_E (with $\omega_E \propto$ plasma density), approaches the applied frequency, ω_{RW}. Good compression is achieved over a broad range of rotating wall frequencies, without the need to tune to a mode in the plasma. The resulting steady-state density is only weakly dependent on the amplitude of the rotating-wall drive. Detailed studies of these states are described, including the evolution of the plasma temperature, peak density, and density profiles during compression; and the response of the plasma, once compressed, to changes in frequency and rotating-wall amplitude. Experiments are conducted in a 4.8 T magnetic field with $\sim 10^9$ electrons. The plasmas have initial and final temperatures of ~ 0.1 eV. They can be compressed to steady-state densities $> 10^{10}$ cm^{-3} and plasma radii < 200 μm. The outward, asymmetry-driven plasma transport rate, Γ_o, of the compressed plasmas is independent of density, n, in contrast to the behavior at lower densities where $\Gamma_o \propto n^2$. The implications of these results for the creation and confinement of high-density electron and positron plasmas and the creation of finely focused beams are discussed. © *2006 American Institute of Physics.* [DOI: 10.1063/1.2179410]

I. INTRODUCTION

There are many uses of trapped single-component plasmas such as in atomic clocks, tailoring positron beams for materials characterization, and the production of low-energy antihydrogen.[1,2] Beyond the applications, these plasmas are interesting in their own right, due in no small part to the fact that they can be prepared and maintained in thermal equilibrium states. Consequently it is important to understand the range of accessible plasma parameters, including the limits on plasma temperature and density, and the factors that limit plasma confinement. Recently we reported a study of torque-balanced steady states of electron plasmas using cyclotron cooling to balance plasma heating and a rotating electric field [i.e., the so-called "rotating wall" (RW) technique] for radial compression and the mitigation of outward transport.[3] In this paper, we describe further studies of these novel plasmas, examining their approach to steady states following compression; and once compressed, the response of these plasmas to further manipulation with RW fields.

A central principle underlying the description of single component plasmas in Penning-Malmberg traps is the fact that, in a strong magnetic field, conservation of angular momentum places a stringent constraint on the evolution of the mean-square plasma radius, namely,

$$P_\theta \approx \frac{-eB_0}{2c} \sum_j r_i^2 \approx -N\frac{eB_0}{2c}\langle r^2 \rangle. \tag{1}$$

In Eq. (1), P_θ the total plasma angular momentum, $-e$ is the electron charge, B_0 is the axial magnetic field, N is the total number of particles (in this case assumed to be electrons), c is the speed of light, r_j are the particle radii, and $\langle r^2 \rangle$ is the mean-square radius of the plasma.[4] Note that Eq. (1) assumes that $\omega_p/\Omega_c \ll 1$, where ω_p is the plasma frequency, and Ω_c is the cyclotron frequency.

The space charge of a single component plasma in a Penning-Malmberg trap produces a radial electric field that causes the plasma to rotate about the magnetic field direction. For a uniform plasma, this rotation is given by the $E \times B$ drift frequency, $\omega_E = 2\pi f_E = \omega_p^2/2\Omega_c = 2\pi nec/B_0$, where n is the plasma density. In an ideal, cylindrically symmetric trap, there are no asymmetries that break the conservation of angular momentum. In practice, torques from small trap asymmetries, either electric or magnetic, drag on the spinning plasma causing the plasma to expand. While this asymmetry-driven expansion is present in all traps, the particular details vary widely depending on the plasma parameters and the nature of the trap asymmetries.[5–7]

The intimate relationship between the angular momentum and plasma radius, expressed in Eq. (1), has lead to the development of a very effective method to radially compress magnetized single-component plasmas. Namely, the application of a torque increases the angular momentum, resulting in a decrease in the radial extent of the plasma. This can be accomplished conveniently and effectively using a rotating

electric field or, for ion plasmas, using the absorption and re-emission of laser light to inject angular momentum.[8] The effectiveness of the technique depends upon the efficiency of coupling of the external torque to the plasma. Since the external agent used to apply the torque does work on the plasma and heats it, an efficient plasma cooling mechanism is required for good compression.

By segmenting a cylindrical trap electrode azimuthally, a properly phased electric field perturbation can be applied that rotates about the trap axis—this has been termed a "rotating-wall" (RW). Rotating-wall fields have been used to compress single-component plasmas in a variety of regimes, including large ion clouds,[9] small ion crystals,[10,11] and electron[12,13] and positron plasmas.[14,15] Generically, the torque from the RW electric field will compress the plasma if the RW frequency, f_{RW}, is larger than the plasma rotation frequency ($f_{RW} > f_E$), and it will cause expansion if it rotates slower ($f_{RW} < f_E$).[16]

If there are no other torques on the plasma, then the plasma will either compress or expand until the plasma rotation frequency matches the applied frequency. This is termed the "no-slip" condition, where the "slip" is given by $\Delta f = f_{RW} - f_E$, namely the difference between the applied RW frequency and the plasma rotation frequency, and the no-slip condition is $\Delta f = 0$. Static trap asymmetries always produce a drag on the plasma causing expansion. In this case, the plasma will achieve a torque-balanced steady state when the torque from the applied RW electric fields equals the drag torque from the trap asymmetries, resulting in $\Delta f > 0$.

The distinguishing feature between previous experiments on RW compression and those described here is the amount of slip observed when compressing the plasma to high-density steady states. Previous work on RW compression of electron plasmas was done in a regime in which the RW fields coupled to Trivelpiece-Gould (TG) modes in the plasma (e.g., see Ref. 13). Specifically, frequencies used were such that $f_{RW} \approx f_{TG} \gg f_E$, where f_{TG} is the frequency of a resonant TG mode. In this case, the slip was large, namely, $\Delta f \approx f_{TG} - f_E > f_E$.[12,13]

The compression experiments reported here are done on electron plasmas in a "low-slip" regime in which the plasma rotation frequency is close to the RW drive frequency ($\Delta f \ll f_E$), a regime in which coupling to plasma modes is unlikely. In this regime, strong cyclotron cooling combined with the weak torque necessary to maintain the compressed plasma results in states weakly perturbed from thermal equilibrium. This raises the possibility that the resulting torque-balanced steady states can be described quantitatively using equilibrium statistical mechanics,[16,17] an idea that we plan to explore further. A similar low-slip regime was described in a study of ion plasmas in the fluid limit very near the transition to solidification.[11] However, a key feature of that work was that the RW electrode covered the entire plasma (i.e., $k_z = 0$), a condition that leads to poor coupling in the experiments described here.

The remainder of this paper is organized as follows. The details of the experimental apparatus and procedures are presented in Sec. II, including a description of the compression experiments. In Sec. III, the observations leading to the identification of the strong-drive regime and its significance are
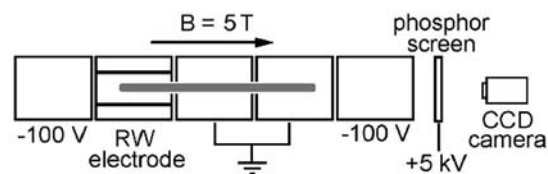

FIG. 1. Schematic diagram of the experiment (not to scale; not all electrodes are shown).

discussed. Section IV describes experiments designed to elucidate different aspects of the strong-drive regime. In Sec. V, the role of transport due to trap asymmetries is discussed. A transport regime is identified that is only weakly dependent on plasma density, and the implications of the existence of this regime for the creation of high-density, torque-balanced steady states is discussed. Section VI contains a discussion of the equations that describe the coupling between RW compression and heating and the important role of strong cyclotron cooling. Section VII presents a discussion of the observed hysteresis in plasma compression and expansion that are observed when varying the RW frequency and the observation of "zero-frequency" trap resonances. The final section of the paper describes plans for future work, such as further elucidation of the RW compression mechanism and the possibility of a near-thermal-equilibrium description of the dynamics of these torque-balanced steady states. The potential importance of these states for selected applications is also briefly discussed.

II. EXPERIMENT DESCRIPTION

The experiments were performed in a cylindrical Penning-Malmberg trap, shown schematically in Fig. 1. Plasmas are confined radially by a 4.8 T magnetic field, with axial confinement provided by voltages (typically −100 V) applied to the end electrodes. The wall diameter is 2.54 cm, and the plasma length, L_p, can be varied in the range $5 \le L_p \le 25$ cm, using different electrode configurations. Electron plasmas are injected using a standard electron gun, with initial plasma radii $R_p \sim 1-2$ mm, and particle numbers, N, in the range $10^8 < N < 10^9$. For ease of comparison, almost all of the experiments presented here had $N \approx 3 \times 10^8$.

Rotating electric fields are applied to the plasma using a special-purpose, four-phase rf generator attached to a four-segment electrode. Each segment extends 90° azimuthally and 2.54 cm axially; combined, they produce a radial electric field with azimuthal mode number $m_\theta = 1$ rotating in the same direction as the plasma. While the rf circuit can operate from 0.1 to 80 MHz, studies, thus far, have been limited to $f_{RW} \lesssim 15$ MHz. While the origin of this limitation is not fully understood, it appears to be related to phase shifts due to electronic resonances associated with the electrode structure and connection circuitry, rather than an intrinsic plasma effect.

The data presented here correspond to the RW electrode located near one end of the plasma column, as shown in Fig. 1, but good confinement and compression have also been achieved with the RW at other locations. Theoretically, an $m_\theta = 1$ rf dipole field applied over the entire plasma can drive

no torque.[16] Although not studied in detail, we find that good compression can be achieved as long as the axial extent of the RW electrode is less than half the plasma length.

The trap is operated in "inject-manipulate-dump" cycles that exhibit very good shot-to-shot reproducibility, typically $\delta N/N \sim 1\%$, where N is the particle number. Density profiles are measured destructively by accelerating the dumped plasmas onto a phosphor screen biased to +5 kV and imaged with a CCD camera (effective pixel size of 12.5 μm in the plasma). The profile is obtained by radially averaging the images about the center of the plasma. Alternatively, the screen can be attached to a charge-to-voltage amplifier for measuring the total charge, N.

To obtain the plasma length, the measured profiles and the particle number, N, are used as inputs to solve the Poisson and Boltzmann equations iteratively for the self-consistent density and potential in r and z.[18] The plasma length can also be estimated by a Gauss' Law measurement and N. This gives an average length, with values that compare well with the average length from the Poisson-Boltzmann calculation. For fixed N, the space charge potential, Φ_0, increases as the plasma is compressed, and so the plasma length changes slightly as a function of density. Typical values of Φ_0 range from 10 V to 80 V.

The parallel plasma temperature, $T_\parallel$, is measured by slowly lowering the confinement voltage and measuring the escaping charge.[19] For the plasmas studied here, the perpendicular-to-parallel equilibration rate is rapid ($\nu_{\perp\parallel} > 1000$ s^{-1}), so $T_\parallel \approx T_\perp \equiv T$.[20] Heat transport is also rapid with the thermal relaxation time $\tau_{th} < 10$ ms;[21] and so we assume the temperature is independent of radius. The plasma cools by cyclotron radiation in the 4.8 T magnetic field at a measured rate $\Gamma_c = (1/T)(dT/dt) \sim 5.9$ s^{-1}.[20,22] This is fast compared to the compression and expansion time scales. Thus, in most cases, the plasmas remain relatively cool (i.e., $T \lesssim 0.2$ eV; $T/e\Phi \ll 1$), even in the presence of strong RW fields.

After the plasma is injected into the trap, the RW field is turned on at frequency f_{RW} and amplitude V_{RW}. The evolution of the plasma is studied by repeating the experiment for different hold times. This is different than previous experiments that utilized frequency ramps.[12] In some experiments, after a given steady-state has been reached, f_{RW} or V_{RW} are changed on a time scale of milliseconds. This is slow compared to particle dynamics (i.e., typical particle bounce and plasma rotation times are 2 μs and 0.3 μs, respectively), but fast compared to the time for the evolution of the plasma. In particular, the rates of temperature and density evolution, dT/dt and dn/dt, are typically longer than 100 ms.

The time-evolution of n and T during RW compression is shown in Fig. 2. Here the central density n_0 is plotted as a function of RW time, where the RW is turned on at $t=0$ s with $f_{RW}=4$ MHz and $V_{RW}=1.0$ V. There are two density data points at each time, and they typically differ by $<1\%$, demonstrating robust compression and the reproducibility of the experiment. Each temperature data point is the average of four measurements, and the error bars represent the typical variation of these data.

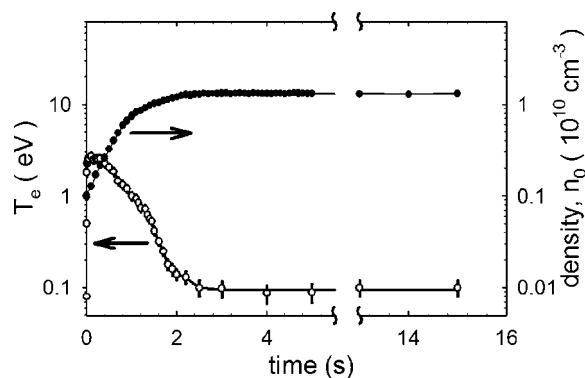Figure 2 shows the evolution of a typical plasma in what

FIG. 2. Central density, n_0 ($\bullet$), and temperature, T_e ($\bigcirc$), as a function of RW time, where the RW is turned on at $t=0$ s with $f_{RW}=4$ MHz, $V_{RW}=1.3$ V, and $L_p \approx 14$ cm. Note the steady-state values, $n_0=1.3 \times 10^{10}$ cm^{-3} and $T_e=0.1$ eV, are reached in less than 3 s and remain constant for more than 10 s. For these experiments, and most of the data in this paper, $N \approx 3 \times 10^8$ electrons.

we identify below as the "strong-drive" regime. The plasma density rises exponentially to a steady-state value, corresponding to a rotation frequency that is very close to the applied frequency. The steady-state density is found to be about 1.3×10^{10} cm^{-3}, which corresponds to $f_E \approx 3.9$ MHz, obtained with a drive of $f_{RW}=4.0$ MHz. In this example the steady-state rotation frequency is only 3% lower than the applied drive frequency. The temperature rises rapidly to about 3 eV in the first 20 ms, levels off, and then drops at an exponential rate comparable to that of the density rise. Note that the time scale for the temperature evolution $[(1/T)dT/dt \sim 1.0$ s$^{-1}]$ is much slower than the cyclotron cooling rate.

The work described below focuses on the evolution of the plasma to high-density steady states, the nature of these states, and the limits that can be achieved. In general, when the plasma reaches such a state, the temperature is relatively low $T \lesssim 0.2$ eV. At early times, a sharp increase in temperature is observed, the magnitude of which increases with both V_{RW} and the initial slip Δf_0, where $\Delta f_0 = f_{RW} - f_{E0}$, and f_{E0} is the plasma rotation frequency at $t=0$. This is followed by a decrease in temperature that occurs on the same time scale as the increase in plasma density, as illustrated in Fig. 2. While not discussed here, this appears to be a consequence of the evolution of the plasma through a sequence of thermal equilibrium states.[16] We believe this is a potentially important aspect of the research and plan to pursue this in further detail in the future.

III. STRONG-DRIVE REGIME

A series of experiments were conducted to investigate the range of achievable plasma parameters utilizing a strong RW drive for various frequencies. The main results, some of which have been described previously,[3] are shown in Figs. 3–5. The behavior illustrated in these figures is typical of "strong-drive" RW compression, namely the quite general tendency for the plasma to reach a steady state in which f_E is very close to f_{RW}.
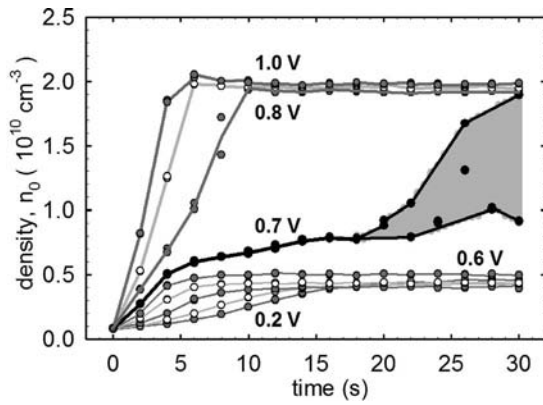
FIG. 3. Time evolution of plasma density for different drive amplitudes for $f_{RW}=6.0$ MHz, and $L_p \approx 14$ cm. Each data symbol differs from the previous by 0.1 V. The lines are guides to the eye. The shaded area signifies the transition region between weak and strong drive.

The transition to this new regime is illustrated in Fig. 3 which shows a series of compression experiments at fixed frequency for different values of the drive amplitude, V_{RW}. For $V_{RW} < 0.7$ V, the plasma is compressed to a limiting density of about 5×10^9 cm^{-3}. However, at $V_{RW}=0.7$ V, there is a bifurcation to a new, high density regime. Namely, after first evolving slowly, the density reaches a point (for $t \gtrsim 18$ s) at which a small change in initial conditions produces a dramatic change in the evolution, the details of which vary from shot-to-shot. Above this RW drive amplitude, the plasma always compresses to a much higher density with n_0 approaching 2×10^{10} cm^{-3}. For values of $V_{RW} > 0.7$ V, the compression rate increases, but this affects only weakly the final steady state.

For fixed large-amplitude drive, plasma compression and steady states are achieved for a range of drive frequencies. This is illustrated in Fig. 4, where the density evolution is shown for drive frequencies of 2, 4, 6, and 8 MHz, with $V_{RW}=1.0$ V. As the frequency increases, the steady-state density also increases. Also shown in Fig. 4 is the character-
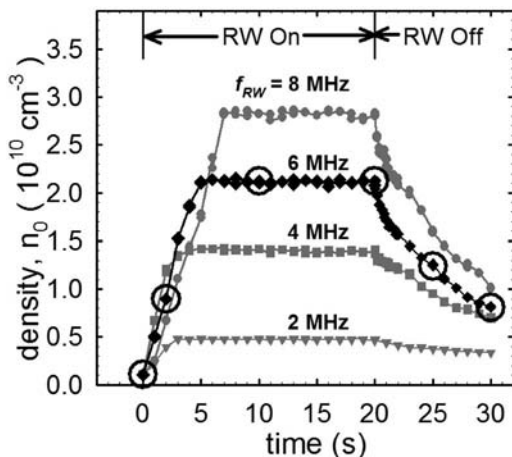

FIG. 4. A series of compression experiments for $L_p=14$ cm and $V_{RW}=1.0$ V for different values of f_{RW} from 2 to 8 MHz. The circles on the 6 MHz data indicate the times at which density profiles are presented in Fig. 6 below.
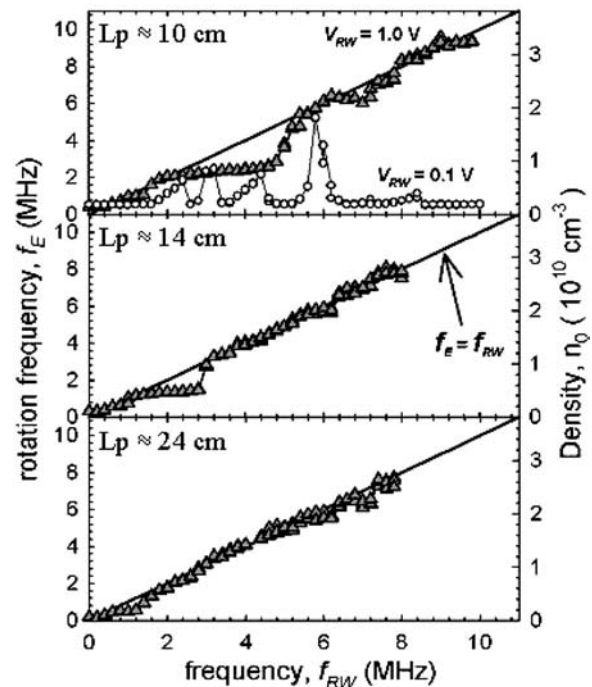

FIG. 5. Steady-state density vs f_{RW} for three different plasma lengths: (▲) $V_{RW}=1.0$ V; and in the top panel, (○) correspond to V=0.1 V. The solid lines are guides to the eye corresponding to $f_{RW}=f_E$.

istic plasma evolution after the RW has been turned off. For the data shown in Fig. 4, at all RW frequencies, the plasma density decreases at a rate much slower than that of the initial compression. This implies that the steady-state RW torque is much less than the initial torque, as suggested by a new theory by O'Neil and Anderson.[23]

To further investigate the frequency dependence, an experiment was performed in which the steady-state density was measured over a broad range of f_{RW} at fixed RW amplitude. The results are shown in Fig. 5, where the steady-state density is plotted versus applied RW frequency, for three different plasma lengths. Note that the vertical scale is given in terms of both density and the plasma rotation frequency, f_E. In the top panel of this plot, data are shown for two values of drive amplitude, $V_{RW}=1.0$ V and 0.1 V, for a plasma length of 10 cm. As expected, in the low-amplitude case, significant compression is observed only near discrete frequencies, likely due to strong coupling to plasma modes, similar to what is described in Ref. 12.

The behavior at large drive amplitude is qualitatively different. For the three different plasma lengths shown in Fig. 5, the data show large ranges of f_{RW} for which strong plasma compression is observed, where the plasma rotation frequency, f_E approaches the RW frequency (i.e., solid lines in Fig. 5). This close matching of the plasma rotation frequency to the drive frequency is what we refer to as "low-slip," i.e., $\Delta f \ll f_E$. The RW heating power delivered to the plasma is proportional to this slip. Hence a low-slip regime implies low power, or alternately low torque, and thus corresponds to a weak drive. In turn, the small heating rate in this regime allows the plasma to evolve to states that closely approximate thermal equilibria. Finally, it should be noted
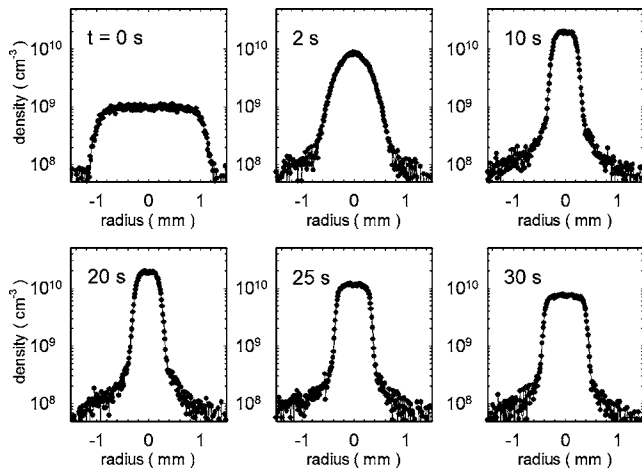
FIG. 6. Radial density profiles are shown during compression and expansion for the times labeled in Fig. 4 for $f_{RW}=6.0$ MHz, $V_{RW}=1.0$ V, and $L_p \approx 14$ cm. The initial plasma ($t=0$ s) is compressed for 20 s and then allowed to expand with the RW off. It should be noted that during the rapid plasma compression (e.g., $t=2$ s), the plasma is quite warm (similar to Fig. 2) and the diamagnetic term in the expression for the rotation frequency is non-negligible. As a consequence, all profiles shown correspond to plasmas close to thermal equilibrium.

that the "steps" in the strong-drive data shown in Fig. 5 are due to coupling of the plasma to a static field asymmetry, as discussed in more detail in Sec. VII.

If the plasma is close to thermal equilibrium, then this should be evident in the observed plasma density profile. As is well known,[16,24] a cold, thermal equilibrium single-component plasma has a radial density profile that is approximately constant out to the plasma edge and then decreases exponentially as a function of radius on the spatial scale of the Debye length, λ_D. Plasmas with $R_p \gg \lambda_D$ closely approximate a "flat-top" density profile. The radial density profiles were investigated for the strong-drive case shown in Fig. 4, with $f_{RW}=6$ MHz, by measuring the density profiles at the times indicated by the circles in that figure. The corresponding density profiles are shown in Fig. 6. Initially, the plasma has a broad, flat-topped distribution, corresponding to a Debye length much smaller than plasma radius (i.e., initially $R_p \gtrsim 10\lambda_D$). Midway through the compression, the plasma density profile is qualitatively different, approaching a Gaussian distribution as a function of radius. This is a manifestation of the increased plasma temperature that occurs during strong compression (e.g., see Fig. 2). When the plasma approaches steady state, the density distribution becomes flat with sharp edges, again indicating a Debye length much smaller than the plasma radius (typically $R_p \sim 10\lambda_D$ in steady state).

The evolution of the plasma density profile, after the RW wall fields are turned off, is quite different. As shown in the bottom half of Fig. 6, the plasma maintains a flat-top density profile during the plasma expansion. It is also evident from Figs. 4 and 6 that the time scale for the plasma decay rate is significantly slower than the plasma compression rate. This is consistent with the idea that, after reaching a steady state, the torque on the plasma is only a weak perturbation.

In Fig. 5, data are shown only up to a maximum fre-

quency of 8–10 MHz, depending on the plasma length. Compression at frequencies as high as 15 MHz have been studied by making discrete increases in f_{RW} on relatively small plasmas, but difficulties were encountered in achieving steady-state plasmas at these higher frequencies. We do not believe this is a fundamental limit of the technique, but rather, as mentioned earlier, a limit of the transmission-line coupling of the drive circuit to the segmented RW electrodes. We believe that these individual, azimuthal segments have slightly different impedances, which causes phase shifts at the higher frequencies. These phase shifts, in turn, produce components to the RW electric fields in addition to $m=1$ (i.e., pure dipole coupling), that cause appreciable plasma heating. The large heating observed at these higher frequencies tends to drive the plasma unstable, inhibiting the achievement of a steady-state plasma.

In general, the strong-drive regime is characterized by relatively rapid plasma compression as compared to the rate of the plasma expansion in the absence of the RW drive (cf. Fig. 4). In this regime, the density increases until there is only a fractionally small difference between the plasma rotation frequency and the RW drive frequency. For example, from the data in Fig. 5, for $L_p \approx 14$ cm, and $f_{RW}=6.0$ MHz, we find $(f_{RW}-f_E)/f_{RW} \lesssim (0.15$ MHz$)/6$ MHz ≈ 0.025, or $\Delta f/f < 3\%$, demonstrating the "low slip" in the strong-drive regime. For the plasmas studied here, the time scales for thermal and momentum transport are small compared to those for compression and cyclotron cooling, and so the plasma remains close to thermal equilibrium, as illustrated by the rigid-rotor profiles shown in Fig. 6.

IV. DYNAMIC EXPERIMENTS

In the previous section, we described the steady-state plasmas that can be created using RW compression in the strong-drive regime. In this section, we describe the dynamic properties of these states. Specifically, we investigate what happens to a torque-balanced steady state in the small slip regime when the RW drive is changed, by either changing the amplitude or the frequency of the drive. To illustrate this behavior, we use as a starting point a state with $f_{RW}=4$ MHz, and $V_{RW}=1.0$ V, corresponding to the black diamonds in Fig. 4.

Shown in Fig. 7 is the dynamic response of the plasma when subject to a change in the drive amplitude. Here the density evolution is shown for a plasma that was initially compressed with $V_{RW}=1.0$ V until $t=15$ s, at which time the drive amplitude was decreased to 0.5, 0.2, and 0 V. An expanded density scale is used to emphasize the relatively small changes in density. As shown by the grey squares, a drop in amplitude by a factor of 2 causes the density to drop by less than 5%. Note (e.g., Fig. 3) that this amplitude is below the transition amplitude corresponding to the strong-drive regime. Namely, the application of this small of an initial drive amplitude to a low density plasma would not compress it to the high density shown in Fig. 7. As shown by the grey circles in Fig. 7, even a factor of 5 smaller drive amplitude is able to maintain the compressed plasma state with a density drop of only ~20%. Thus the plasma exhibits
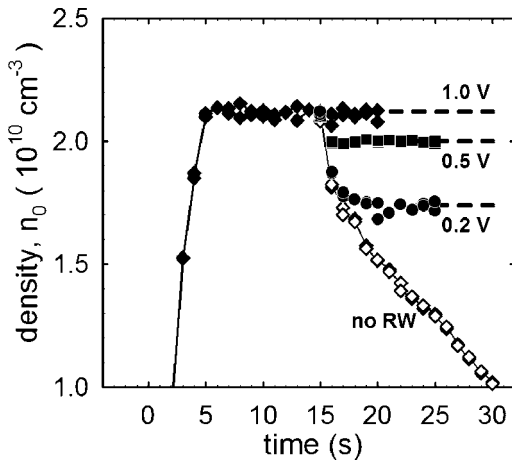
FIG. 7. Investigation of the change to the steady-state density when V_{RW} is changed for $f_{RW}=6.0$ MHz. Note that the density scale has been changed in order to make the decrease in density more apparent. Also note that a factor of 2 drop in V_{RW} only caused a 5% drop in the density.

very significant hysteresis as a function of the applied RW amplitude. This hysteresis, is another demonstration of the difference between strong- and weak-drive compression.

Shown in Fig. 8 is a study of the plasma dynamics after a change in the drive frequency. Here the same 6 MHz, 1 V evolution is followed for the first 15 s. Then at $t=15$ s, f_{RW} is changed to 8 MHz (up triangles) and 4 MHz (down triangles). For comparison, the dashed lines indicate the respective steady-state densities achieved if these frequencies were applied directly as in Fig. 4. The data show that the plasma evolves very rapidly to match the new drive frequency. Note that the time scale is very rapid, namely, $t_{eq} < 1$ s, as compared to the initial compression for which $t_{eq} \sim 5$ s.

The evolution of the plasma as a result of a frequency change is investigated further in Fig. 9 for a plasma that was initially compressed with $f_{RW}=8$ MHz and $V_{RW}=1.0$ V. Figure 9(a) shows the time evolution when the drive is changed at $t=0$ to the frequencies indicated in the figure. As is evident from the curves for $f_{RW} \leqslant 5$, the time required to achieve the
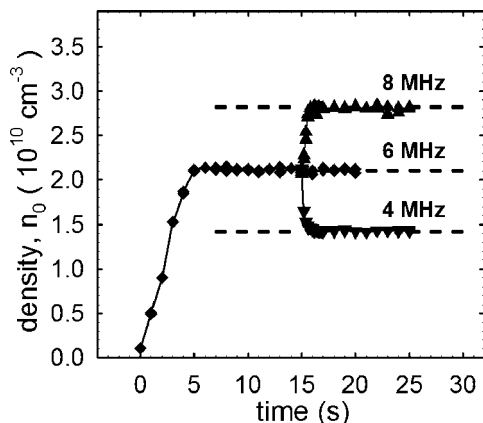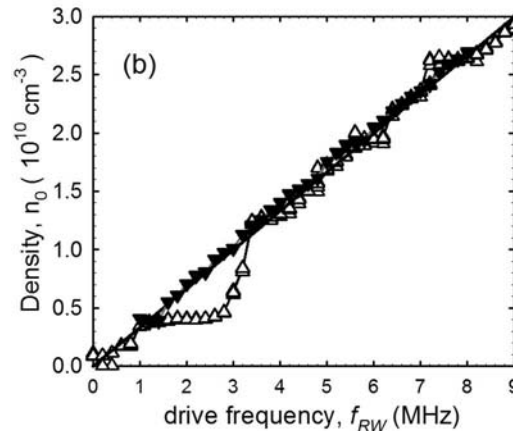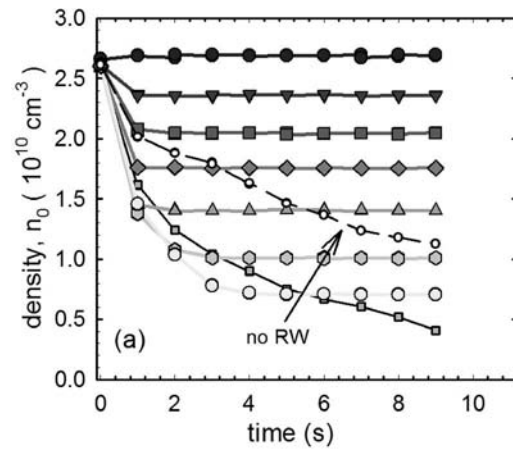

FIG. 9. (a) Density vs time when f_{RW} is dropped. The lines are guides to the eye. Note that the change in frequency causes a rapid change to the new equilibrium, typically much faster than the plasma expansion with no RW. (b) Steady-state density ($\blacktriangledown$) when f_{RW} is abruptly decreased from 8.0 MHz, as in Fig. 9(a), over a broad range of f_{RW}. Also shown are data from Fig. 5 ($\triangle$) over the same range in f_{RW}, applying a fixed frequency to compress the plasma to the final steady-state density. For all data shown, $L_p \approx 14$ cm.

new equilibria are much faster than the plasma expansion time, labeled "no RW" in Fig. 9(a). This indicates that, for these frequency changes, the RW torque is much larger than the steady-state torque. This indicates that the torque is proportional to the slip Δf, which is large during the evolution and becomes small as the plasma approaches steady state.

The response of the plasma to the application of different values of f_{RW} over a broad range in frequency is shown in Fig. 9(b). Here the steady-state density is plotted for f_{RW} applied directly (i.e., Fig. 5), and after first compressing to steady-state using $f_{RW}=8$ MHz and then reducing f_{RW} as shown in Fig. 9(a). The observed "step" is only apparent when approached via plasma compression and is not seen during plasma expansion. This is a second type of hysteresis observed in the strong-drive regime and is discussed further in Sec. VII. With the exception of this step, any density can be accessed by application of the corresponding value of f_{RW}, and once accessed, states with a different density can be accessed by changing the drive frequency.

We finish our investigation of the dynamic behavior in the strong-drive regime by investigating the robustness and repeatability of the compression process. Shown in Fig. 10 is

FIG. 8. Investigation of the change in steady-state density produced when f_{RW} is changed at $t=15$ s to 4 ($\blacktriangledown$) and 8 MHz ($\blacktriangle$) for $V_{RW}=1.0$ V and an initial f_{RW} of 6 MHz. The dashed lines indicate the steady-state density achieved when f_{RW} is applied directly, as in Fig. 4.
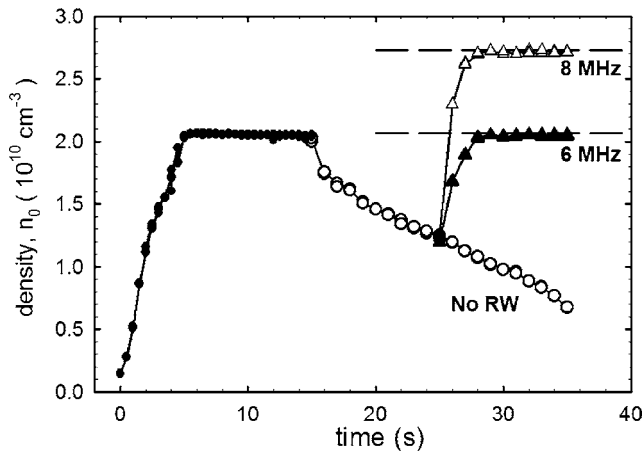
FIG. 10. Density vs time for a series of compression experiments as an example of robust plasma compression. Initial compression (●) with f_{RW} =6.0 MHz and V_{RW}=1.0 V is followed by expansion with the RW off (○), then compressed again with f_{RW}=6 (▲) and 8 (▽) MHz. The dashed lines indicate the steady-state density achieved when the final value of f_{RW} is applied directly, as in Fig. 4.

the plasma response after cycling the RW field off, allowing the plasma to expand, then compressing to a new torque-balanced, low-slip steady state. The plasma was first compressed with f_{RW}=6 MHz and V_{RW}=1.0 V for 15 s, similar to the process illustrated in Figs. 7 and 8. Then the drive is turned off for 15 s<t<25 s, and the plasma is allowed to expand. At t=25 s, the drive is turned back on with either f_{RW}=6 or 8 MHz. As before, the dashed lines indicate the density to which the plasma would have evolved if that frequency were applied directly. Even though significant expansion has occurred ($n \sim n_0/2$), RW compression brings the plasma back to the same torque balanced state as if the free expansion phase had not occurred.

This compression, expansion, compression cycle can be repeated many times (e.g., >50 cycles; not shown) with <1% degradation of the plasma total charge, a fluctuation level equivalent to the shot-to-shot noise. Thus these torque-balanced low-slip states exhibit "robust" compression over a broad range of frequencies, very different than that which would be observed if the coupling were to a specific mode. In a separate experiment, we have held a plasma in a high-density, compressed steady state for over 24 h with <1% change in the density. Further experiments are planned to explore the very long time (e.g., day and week) compression and storage of plasmas in this strong-drive regime.

V. EVIDENCE FOR A NEW TRANSPORT REGIME

Two torques are operating on the plasma in the compression experiments described above, the RW drive torque, $\mathcal{T}_{RW}$, and the drag torque, $\mathcal{T}_a$, that is assumed to be due to trap asymmetries. Observation of the plasma expansion with the RW fields off provides a measure of the asymmetry-induced drag torque (e.g., Fig. 4). Consequently, rotating-wall compression, followed by "free" expansion, can provide a measure of the drag torque over a wide range of plasma densities.

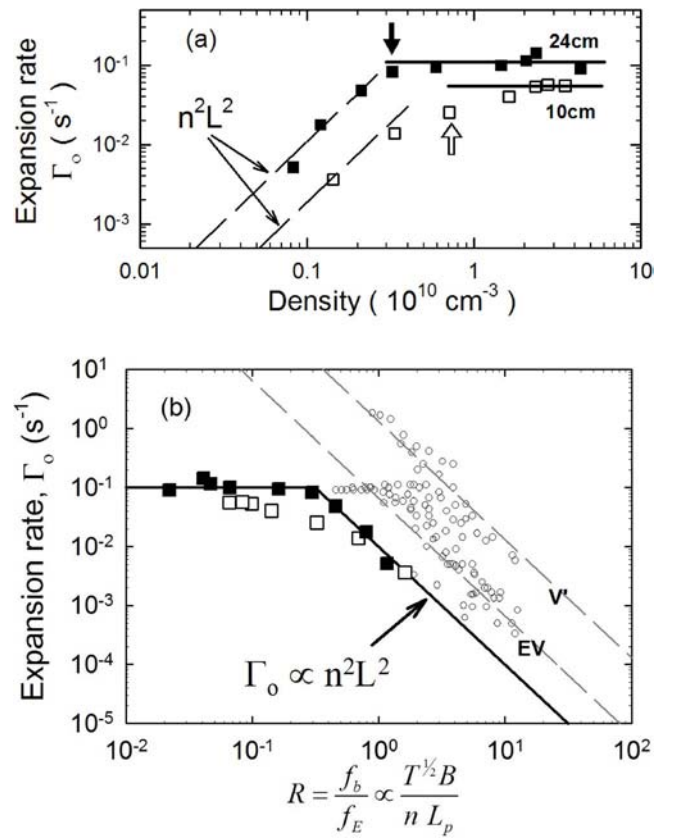Figure 11(a) shows the measured asymmetry-induced expansion rate, Γ_o, for two plasma lengths and a range of

FIG. 11. (a) Outward asymmetry-induced transport vs plasma density for two different plasma lengths, L_p=24 cm (■), and 10 cm (□). Vertical arrows correspond to the densities at which $\nu_c=3f_b$. (b) Outward asymmetry-induced transport vs plasma "rigidity," where $R=f_b/f_E$. The square data points are the same as in Fig. 11(a). Small hollow circles are from Ref. 25. The dashed lines labeled V' and EV are from Ref. 26.

plasma densities. The asymmetry transport has been shown to scale as $\Gamma_o \sim f_E^2/f_b^2 \sim n^2 L_p^2$.[25] This implies that, as the density increases, the drag does also; and for low densities $(10^8 – 10^9)$, $\Gamma_o \propto n^2$. However, the data in Fig. 11(a) indicate that, for densities $n \gtrsim 10^{10}$, the transport rate is only weakly dependent on plasma density, if at all. As shown in Fig. 11(b), similar behavior has been observed previously in other high-density and/or cold plasmas.[13,25]

The origin of this change in scaling of the transport with density is presently unclear. This is perhaps not surprising, since understanding asymmetry-driven transport in single-component plasmas has proven to be exceedingly challenging; and a complete, predictive theory has yet to be developed.[7,27] We note that the change in density scaling occurs when the collision frequency becomes comparable to the axial bounce frequency, namely the arrows in Fig. 11(a) show where $\nu_c \sim 3f_b$, where ν_c is the electron-electron collision frequency. This signals the transition from the regime where bounce resonances can be important to one in which the particles diffuse along field lines, and this could affect the magnitude of the outward transport. We note that, for these experiments, this condition also corresponds to $f_E \sim 3f_b$. It is presently unclear which, if either, of these criteria is related to the observed change in the density scaling of Γ_o.

This change in density scaling may be one reason previ-

ous electron experiments did not observe the strong-drive behavior reported here, since in these other experiments, the asymmetry-driven transport was in the $\Gamma_o \propto n^2$ regime.[13] In the latter case, the torque necessary to balance the outward transport increased with increasing density. This implies that the necessary slip to balance the drag would become larger as the density increased. This, in turn, would further increase the plasma temperature, decreasing the collision frequency, possibly inhibiting the plasma from entering the strong-drive regime.

It is also possible that it is the magnitude of the asymmetry drag that is more important than the scaling of Γ_o with density in enabling strong-drive operation. For the lower frequency data in Fig. 5, f_E is still quite close to f_{RW} even though this is in the $\Gamma_o \propto n^2$ regime. In this context, previous experiments, which did not observe the change in density scaling, did not have as strong cooling as the experiments reported here.[13] As discussed in the next section, the larger plasma heating associated with the larger transport may have been a more critical issue in previous experiments. It remains to be seen whether the more benign scaling, $\Gamma_o \propto n^0$, is crucial to strong-drive operation or is a coincidence.

VI. TRANSPORT AND HEATING IN TORQUE-BALANCED STEADY STATES

The measurements described above can be used to investigate the relationship between compression and plasma heating, regardless of the physical origin of the asymmetry-induced drag torque, $\mathcal{T}_a$. To maintain the compressed state, the applied rotating fields must inject angular momentum at a rate that balances the effect of the outward expansion. In the following, we make the crucial assumption that the outward transport rate, Γ_o, and hence the asymmetry torque, $\mathcal{T}_a$, do not change when the RW fields are on. Thus the free expansion measurements of $\mathcal{T}_a$ can be used as a measure of the applied RW torque.

Noting that $n = N / \pi R_p^2 L_p$, and for a rigid-rotor, $\langle r^2 \rangle \approx \frac{1}{2} R_P^2 = (N/2\pi L)/n$, the time derivative of Eq. (1) can be written,

$$\frac{dP_\theta}{dt} = -N \frac{eB}{2c} \frac{d}{dt} \langle r^2 \rangle \approx \left(\frac{e^2 N^2}{2L_p} \right) \frac{1}{\omega_E} \left(\frac{1}{n} \frac{dn}{dt} \right). \qquad (2)$$

Since $(1/n)(dn/dt) = \Gamma_o$, we write

$$\mathcal{T}_a = \frac{dP_\theta}{dt} \approx \left(\frac{e^2 N^2}{2L_p} \right) \frac{\Gamma_o}{\omega_E}. \qquad (3)$$

There is a one-to-one correspondence between the injected angular momentum and the work done on the plasma,[28] specifically,

$$P_H = \omega_{RW} \mathcal{T}_{RW}. \qquad (4)$$

Assuming that the plasma is in a torque-balanced state, the heating rate can be estimated from the measured expansion rate. From the balance of torques, $\mathcal{T}_a = \mathcal{T}_{RW}$, thus

$$P_H = \left(\frac{e^2 N^2}{2L_p} \right) \frac{\omega_{RW}}{\omega_E} \Gamma_o \approx \left(\frac{e^2 N^2}{2L_p} \right) \Gamma_o, \qquad (5)$$

which assumes the low-slip approximation for the steady state, namely $\omega_{RW} \approx \omega_E$.

The rate of thermal energy increase, P_T, is equal to the difference between the RW heating rate [i.e., P_H from Eq. (5)], and the cyclotron cooling power. Specifically,

$$P_T = P_H - P_c, \qquad (6)$$

where

$$P_T = \frac{3}{2} N \frac{dT_e}{dt}, \qquad (7)$$

T_e is the electron plasma temperature, and

$$P_c = \frac{3}{2} N \Gamma_c (T_e - T_W), \qquad (8)$$

is the cyclotron cooling power with T_W equal to the ambient electrode temperature ($T_W \approx 25$ meV). In steady state, $dT_e / dt = 0$, and Eq. (6) can be solved for the equilibrium temperature, T_{eq}, namely

$$T_{eq} = T_W + \left(\frac{Ne^2}{3L_p} \right) \frac{\Gamma_o}{\Gamma_c}. \qquad (9)$$

For the data shown in Fig. 4, $\Gamma_o \approx 0.1$ s^{-1}, $\Gamma_c \approx 5.9$ s^{-1}, $N \approx 3 \times 10^8$, $L_p \approx 14$ cm, and Eq. (9) yields $T_{eq} \approx 0.05$ eV. This is about a factor of 2 less than the measured plasma temperature.

The measured steady state temperature observed is typically a factor of 2 or 3 times more than the simple estimate above. It is likely that this is due to excess heating by the RW fields, since there are many mechanisms by which oscillating potentials can heat a plasma without changing the angular momentum.[29] As mentioned earlier, previous experiments worked at a lower magnetic field with plasmas that had larger transport rates.[13] In that case, Eq. (6) predicts an equilibrium temperature approximately a factor of 10 larger. As stated above, this likely prevented those experiments from entering the strong-drive, low-slip regime reported here.

VII. HYSTERESIS AND ZERO-FREQUENCY MODES

While application of large-amplitude RW fields typically results in a low-slip final state, there are exceptions, that appear as "steps" in the data shown, for example, in Fig. 5. Similar effects have been observed and studied previously in strongly coupled ion plasmas subject to laser torques.[30] These steps appear to be due to a static asymmetry in the lab frame that drives a mode rotating opposite to the plasma, thereby producing a drag.

In the limit of a cold plasma with $R_p \ll R_w$, and thus $\omega_{TG} \ll \omega_p$, the dispersion relation for Trivelpiece-Gould modes in a single-component plasma can be written (e.g., Ref. 13),
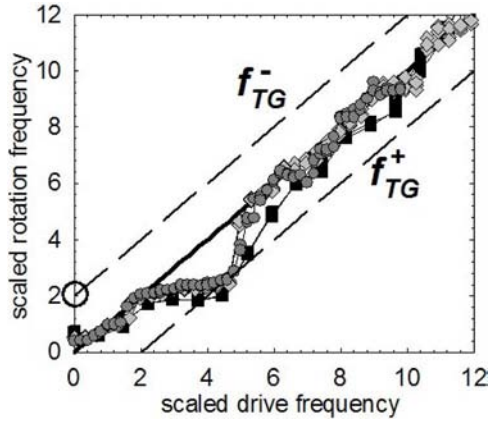
FIG. 12. Scaled plasma rotation frequency is shown as a function of scaled RW drive frequency. Data from Fig. 5 are plotted with all frequencies scaled by $L_p^{3/2}$. $L_p = (\bullet)$ 10 cm; ($\blacktriangledown$) 14 cm; and ($\blacksquare$) 24 cm. The dashed lines are from Eq. (10).

$$\omega_{TG} \simeq m_\theta \omega_E \pm A \omega_p k_z R_p. \tag{10}$$

Here, $m_\theta > 0$, $A = 1/j_{m_\theta n_r}$, with $j_{m_\theta n_r}$ given by $J_{m_\theta}(j_{m_\theta n_r}) = 0$, where J_{m_θ} is a Bessel function. In particular, there exists a value of ω_E, and hence a density,

$$m_\theta \omega_E^o \approx A \omega_p k_z R_p, \tag{11}$$

which gives $\omega_{TG}^- \approx 0$ and $\omega_{TG}^+ \approx 2\omega_E$. Thus if there exists a static (i.e., zero-frequency) trap asymmetry with a given m_θ and k_z, the plasma will become resonant with that asymmetry as the plasma rotation frequency approaches ω_E^o. Noticing that $\omega_p \propto n^{1/2} \propto (N/R_p^2 L_p)^{1/2}$, we find that $\omega_E^0 \propto N^{1/2}/L_p^{3/2}$.

As seen in Fig. 5, the steps appear at a lower density for longer plasma lengths. In Fig. 12, the prediction that $\omega_E^o \propto 1/L_p^{3/2}$ is used to rescale both the drive and rotation frequencies for the data in Fig. 5. The dispersion relation from Eq. (9) is also shown as the dashed lines. The circled point shows the location of the "zero-frequency" mode, i.e., the density at which $\omega_E = \omega_E^o$. When scaled with the changes in length, all of the "steps" collapse to a single curve. This result can be explained by assuming that, when the steady-state plasma density gets close to the zero-frequency resonance, the drag torque from inherent trap asymmetry increases, and the RW torque cannot overcome it. However, when the RW drive approaches the frequency of the f_{TG}^+ mode, the RW drive becomes resonant with this mode and is able to overcome the drag torque, allowing the compression to continue.

In contrast to this behavior, when the rotation frequency is decreased [i.e., as in Fig. 9(b)], the plasma does not encounter this resonance until $\omega_{RW} = \omega_E^o$. Thus the presence of the "steps," such as those shown in Figs. 5 and 12 are evidence of a zero-frequency resonance due to a static asymmetry in the lab frame. As a consequence, it only affects the plasma when the plasma rotation frequency approaches the RW frequency from below.

VIII. SUMMARY AND A LOOK TO THE FUTURE

In this paper we have described a new class of torque-balanced steady states of single-component (i.e., electron or positron) plasmas that can be created using strong RW drive and strong cyclotron cooling. Tuning to a plasma mode is not required for compression, and in fact, would likely be deleterious. The limiting density corresponds to a "low-slip" condition in which the plasma rotation frequency is very close to the applied RW frequency. Plasmas can be compressed into a regime in which outward, asymmetry-induced transport no longer increases rapidly with plasma density. The observed radial profiles and estimates of the thermal and momentum transport and heating rates indicate that these states are approximately uniform-temperature, rigid rotors.

One important, but as yet unanswered question is the maximum density that can be achieved using this technique. Since the observed transport does not increase rapidly with density in this regime, plasma heating will likely not be a limiting factor as it would be in the regime where $\Gamma_o \propto n^2$.[31] The current limit on RW frequency (and hence plasma density) appears to be due to extrinsic resonances in the RW electrical circuit.

The robust, virtually ubiquitous nature of the observed compression indicates that a relatively simple model of the RW torque should be possible. Work along these lines is in progress.[23] In particular, we seek to understand the nature of the torque as a function of RW drive voltage and slip frequency by perturbing the system about the low-slip steady state as, for example, illustrated in Figs. 7 and 8. From a theoretical perspective, in the language of nonlinear dynamics, the present working hypothesis is that both the low-drive (high-slip) and the strong-drive (low-slip) states are stable fixed points for some range of parameters. Above a certain RW drive amplitude and with strong cooling, we believe that the low-drive fixed point becomes unstable and the system is then attracted to the low-slip, near-thermal-equilibrium fixed point.

The fact that the steady-state plasma has a profile close to what is expected for a thermal equilibrium indicates that thermodynamics might be useful in understanding the coupling between density, temperature, and torque.[16] If so, the coupled evolution equations for the plasma temperature and density might be used to calculate the net torque on the plasma as it evolves during compression between the low- and high-slip steady states.

The new RW compression regime reported here can be expected to be of considerable practical importance in tailoring antimatter (e.g., positron) plasmas for a range of applications, such as creating dense antimatter plasmas to study the positronium molecule (Ps$_2$), Bose condensed Ps gases, and the creation of large quantities of cold antihydrogen. Other applications include the brightness enhancement of trap-based positron beams,[32] the development of multicell traps for massive and long-term positron storage,[31] and eventually portable antimatter traps. The plasmas studied here are nearly optimum for such applications. These plasmas can be confined and compressed without tuning to plasma modes, which facilitates compression and multicell operation. In addition, the reduced transport in the high-density regime reduces plasma heating, thereby greatly reducing the requirements for plasma cooling.

ACKNOWLEDGMENTS

[1] C. M. Surko and R. Greaves, Phys. Plasmas **11**, 2333 (2004).

[2] T. M. O'Neil, Phys. Today **52**, 24 (1999).

[3] J. R. Danielson and C. M. Surko, Phys. Rev. Lett. **94**, 035001 (2005).

[4] T. M. O'Neil, Phys. Fluids **23**, 2216 (1980).

[5] J. M. Kriesel and C. F. Driscoll, Phys. Rev. Lett. **87**, 135003 (2001).

[6] J. Notte and J. Fajans, Phys. Plasmas **1**, 1123 (1994).

[7] A. A. Kabantsev, J. H. Yu, R. B. Lynch, and C. F. Driscoll, Phys. Plasmas **10**, 1628 (2003).

[8] J. J. Bollinger, D. J. Wineland, and D. H. E. Dubin, Phys. Plasmas **1**, 1403 (1994).

[9] X.-P. Huang, F. Anderegg, E. M. Hollmann, C. F. Driscoll, and T. M. O'Neil, Phys. Rev. Lett. **78**, 875 (1997).

[10] X.-P. Huang, J. J. Bollinger, T. B. Mitchell, and W. M. Itano, Phys. Rev. Lett. **80**, 73 (1998).

[11] X.-P. Huang, J. J. Bollinger, T. B. Mitchell, W. M. Itano, and D. H. E. Dubin, Phys. Plasmas **5**, 1656 (1998).

[12] F. Anderegg, E. M. Hollmann, and C. F. Driscoll, Phys. Rev. Lett. **81**, 4875 (1998).

[13] E. M. Hollmann, F. Anderegg, and C. F. Driscoll, Phys. Plasmas **7**, 2776 (2000).

[14] R. G. Greaves and C. M. Surko, Phys. Rev. Lett. **85**, 1883 (2000); Phys. Plasmas **8**, 1879 (2001).

[15] L. V. Jorgensen *et al.* (ATHENA Collaboration), Phys. Rev. Lett. **95**, 025002 (2005).

[16] D. H. E. Dubin and T. M. O'Neil, Rev. Mod. Phys. **71**, 87 (1999).

[17] T. M. O'Neil and D. H. E. Dubin, Phys. Plasmas **5**, 2163 (1998).

[18] E. H. Chao, R. C. Davidson, S. F. Paul, and K. S. Fine, in Proceedings of the 1999 Workshop on Non-Neutral Plasmas (Princeton University Press, Princeton, 1999); American Institute of Physics Conference Proceedings, No. 498, edited by J. Bollinger, R. C. Davidson, and R. Spencer (AIP, Melville, New York, 1999), p. 461.

[19] D. L. Eggleston, C. F. Driscoll, B. R. Beck, A. W. Hyatt, and J. H. Malmberg, Phys. Fluids B **4**, 3432 (1992).

[20] B. R. Beck, J. Fajans, and J. H. Malmberg, Phys. Rev. Lett. **68**, 317 (1992).

[21] D. H. E. Dubin and T. M. O'Neil, Phys. Rev. Lett. **78**, 3868 (1997); E. M. Hollmann, F. Anderegg, and C. F. Driscoll, Phys. Plasmas **7**, 1767 (2000).

[22] T. M. O'Neil, Phys. Fluids **23**, 725 (1980).

[23] T. M. O'Neil and M. W. Anderson, Bull. Am. Phys. Soc. **50**, 171 (2005).

[24] S. A. Prasad and T. M. O'Neil, Phys. Fluids **22**, 278 (1979).

[25] B. P. Cluggish, Ph.D. thesis, University of California, San Diego (1995).

[26] C. F. Driscoll and J. H. Malmberg, Phys. Rev. Lett. **50**, 167 (1983); C. F. Driscoll, K. S. Fine, and J. H. Malmberg, Phys. Fluids **29**, 2015 (1986).

[27] D. L. Eggleston and T. M. O'Neil, Phys. Plasmas **6**, 2699 (1999).

[28] R. W. Gould, in Proceedings of the 1999 Workshop on Non-Neutral Plasmas (Princeton University Press, Princeton, 1999); American Institute of Physics Conference Proceedings, No. 498, edited by J. Bollinger, R. C. Davidson, and R. Spencer (AIP, Melville, New York, 1999), p. 170.

[29] B. P. Cluggish, J. R. Danielson, and C. F. Driscoll, Phys. Rev. Lett. **81**, 353 (1998).

[30] D. J. Heinzen, J. J. Bollinger, F. L. Moore, W. M. Itano, and D. J. Wineland, Phys. Rev. Lett. **66**, 2080 (1991).

[31] C. M. Surko and R. G. Greaves, Radiat. Phys. Chem. **68**, 419 (2003).

[32] R. G. Greaves and C. M. Surko, Nucl. Instrum. Methods Phys. Res. B **192**, 90 (1996).